ELSEVIER

Journal of Hydrology 210 (1998) 1–10

Journal of Hydrology

The influence of heat conduction on evaporation from sunken pans in hot, dry environment

I.M. Oroud*

Environmental Fluid Dynamics Program, Department of Mechanical and Aerospace Engineering, Arizona State University, Tempe, AZ 85287-6106, USA

Received 27 May 1997; accepted 24 April 1998

Abstract

Lateral heat conduction across a large circular sunken pan located in a hot, dry environment is evaluated using a numerical procedure. Heat flow across the sunken pan–adjacent soil boundary is calculated using a two-dimensional soil plane. Calculations show that a large temperature differential across the pan–substrate boundary develops during the entire diurnal cycle during January and July, leading to consistently positive heat flow from the soil towards the sunken pan. Heat conduction across the pan–substrate boundary represents 10 and 34% of net radiation over the sunken pan during July and January, respectively. This additional heat source, which is not available for shallow lakes, increases annual evaporation from the sunken pan by about 5–8% in July and January, respectively. In hot arid environments, a sunken pan will overestimate evaporation from a nearby shallow lake/dam due to a larger surface roughness and consistently positive conduction heat flow across the pan–substrate boundary. © 1998 Elsevier Science B.V. All rights reserved.

Keywords: Sunken pans; Evaporation; Shallow lakes; Hot arid environments; Dead Sea; Lake-pan evaporation ratio; Class A pans

1. Introduction

Large scale water harvesting techniques are currently employed in many countries in the Middle East and North Africa due to water scarcity and rapid population growth. Numerous dams and shallow lakes have been constructed in recent years over small rivers and desert wadies to catch overland flow, which occurs mainly in the cold season of the year. These dams, which are usually shallow and cover several km^2, are used either directly for surface irrigation or to recharge underground water. Thus, reliable evaporation data are indispensable for planning, designing and operating reservoirs, particularly in arid and semiarid areas where water resources are very scarce.

Several pan types, which differ in their size, shape, and exposure, have been used to estimate irrigation requirements and water loss from lakes and reservoirs. Class A pans are widely used to approximate lake evaporation (Ferguson et al., 1985). The annual ratio of lake to Class A pan (E_L/E_p) is reported to vary from 0.6 in arid and semiarid environments to around 0.8 in humid environments (Sellers, 1965; Turk, 1970; Brutsaert, 1982). However, the evaporation ratio was found to vary from year to year and for the same month. Although Class A pans are easy to operate and maintain, evaporation rates from sunken pans have been reported to resemble those from shallow lakes encountering identical meteorological forcings

* Present address: Department of Physical Geography, Mu'tah University, Kerak, Jordan. E-mail: ioroud@mutah.edu.jo

0022-1694/98/$ - see front matter © 1998 Elsevier Science B.V. All rights reserved.
PII S0022-1694(98)00153-X

(Kohler, 1954; Hounam, 1973). Compared to Class A pans, large sunken pans have the advantage of disturbing airflow less and having thermal characteristics similar to those of shallow lakes. Kohler (1954) reported that the evaporation ratio of lake to a large sunken pan (E_L/E_S) is generally about 0.9. Sunken pans are currently operated in many countries in the Middle East and North Africa for monitoring evapotranspiration, and as such water requirements for irrigation purposes. The use of these sunken pans can be extended to evaluate evaporation from existing or proposed dams. This is true when field measurements of meteorological forcings are not available, and/or climatological data are of poor quality.

Although evaporation rates from deep sunken pans and shallow lakes/dams do not differ significantly in humid regions, the difference can be important in arid and semiarid areas where the subsurface temperatures are larger than those of sunken pans during the entire diurnal cycle in summer and winter. Field observations and numerical techniques suggest that subsurface heat flux is substantially influenced by surface conditions such as wetness and the presence of vegetation debris. In humid regions the presence of soil moisture, vegetation and organic residues restrict subsurface heat flux substantially (Loomis and Hsiao, 1992; Asaeda and Vu Thanh, 1993; Grant et al., 1995); subsurface heat flux is reported to be around 10% of daily net radiation (Holtslag and Van Ulden, 1983). Thus, it appears very likely that heat conduction in humid environments is of little significance to the energy budget of a sunken pan due to the reduced temperature differential between the pan and the adjacent soil profile. On the other hand, Idso et al. (1975) and Doll et al. (1985) indicate that daily subsurface heat flux is quite pronounced over dry surfaces, reaching 35–40% of daytime net radiation. These findings suggest that subsurface heating in arid environments is an important element in the partitioning of net radiation over the interface, and as such would enhance heat flow across the substrate–pan boundary. This is illustrated in Fig. 1, which shows the integrated average subsurface temperatures (10 to 100 cm), along with those of a large circular sunken pan, 0.9 m deep and with a radius of 1.82 m, observed at the southern edge of the Dead Sea. The temperature difference between the two media is quite pronounced, particularly in summer in which the departure is around 7 K. Thus, heat transport via lateral conduction across the substrate–pan boundary is expected to represent an additional heat source to the sunken pan, thereby increasing evaporation from it. This heat source is not available for shallow lakes because lateral conduction is practically zero, considering the lake area and its perimeter. Therefore, the objectives of this investigation are: (1) to characterize the effect of lateral heat conduction across the subsurface–pan boundary on evaporation from sunken pans, and (2) to illustrate the linkage between evaporation from sunken pans and small lakes/dams located in arid and semiarid environments. This investigation is accomplished using a numerical procedure. The calculations are performed using the environmental conditions prevailing at the southern edge of the Dead Sea.

2. Theoretical considerations

The heat balance of a fully mixed sunken pan can be described in the following form:

$$h_w C_w \frac{\partial T_{pan}}{\partial t} = S(1-a_p) + L_D + \varepsilon_w \sigma T_{pan}^4 - Q_H - Q_E - Q_C \quad (1)$$

where h_w is water depth (m), C_w is the volumetric

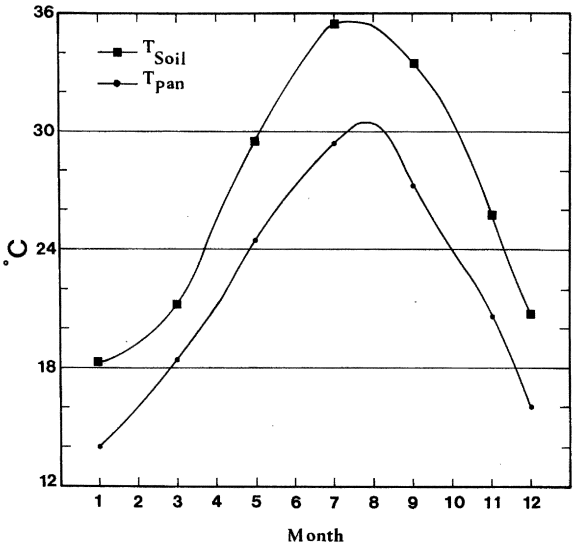

Fig. 1. Long-term depth averaged soil temperature versus sunken pan temperature during the various months of the year.

heat capacity of water (J K^{-1} m^{-3}), T_{pan} is pan temperature (K), t is time, S is global solar radiation reaching the surface of the pan (W m^{-2}), a_p is shortwave albedo, L_D is downcoming longwave radiation (W m^{-2}), ε_w is water emissivity, σ is Stefan Boltzmann constant (5.667×10^{-8} W m^{-2} K^{-4}), Q_H and Q_E represent sensible and latent heat fluxes between the pan and the contiguous atmosphere (W m^{-2}), and Q_C is heat conduction across the substrate–pan boundary (W m^{-2}). The various terms appearing in Eq. (1) are defined below (see also Table 1).

Global solar radiation reaching the surface is evaluated using a model proposed by numerous investigators (Paltridge and Platt, 1976; Iqbal, 1983),

$$S = S_o R^{-2}[\tau_o \tau_r - a_w]\tau_a \cos\theta + S_d \quad (2)$$

where S_o is extraterrestrial solar radiation, R is earth-sun vector ratio, τ_o, τ_r and τ_a, are the corresponding expressions for atmospheric transmittance after attenuation by ozone, Rayleigh scattering, and aerosols, respectively; a_w is solar radiation absorption via water vapor in the troposphere, S_d and θ are diffuse radiation and the zenith angle of the sun, respectively. Diffuse radiation, which represents the contribution of Rayleigh scattering, aerosols and multiple reflection between the ground and the atmosphere, is calculated based on a model presented by Iqbal (1983). Downcoming longwave radiation emitted by the atmosphere is calculated using a semi empirical expression derived by Brutsaert (1975),

$$L_D = 0.553\, e_a^{1/7} \sigma T_a^4 \quad (3)$$

where e_a and T_a are water vapor pressure (mb) and air temperature (K) at the screen level, respectively.

Assuming similarity of turbulent transfers, sensible and latent heat fluxes across the surface–atmosphere boundary are evaluated using the following expression (e.g. Sweers, 1976; Mahrt and Ek, 1984; Arya, 1988):

$$Q_H = \rho C_p k^2 u (T_{pan} - T_a)/(\ln(z/z_o))^2 \phi_h^{-1} \quad (4)$$

$$Q_E = (1/\psi)\rho C_p k^2 u (e_{pan} - e_a)/(\ln(z/z_o))^2 \phi_h^{-1} \quad (5)$$

where Ψ is the psychrometric constant (C_p P/0.622 L_e), ρ is air density, C_p is specific heat of air at constant pressure, u is wind speed, T_{pan} is the pan temperature, e_{pan} is saturation vapor pressure at pan temperature, computed using Teten's formulation (Kimball, 1981), e_a is ambient water vapor pressure, k is von Karman constant (0.4), z_o is surface roughness; and ϕ_h is a measure of the departure from atmospheric neutrality, evaluated using the Richardson's number (Ri).

During unstable conditions (Ri $<$ 0), the departure from atmospheric neutrality (ϕ_h) is evaluated from the following expression (Arya, 1988),

$$\phi_h = (1 - 15\mathrm{Ri})^{-1/2} \quad (6)$$

Under stable conditions (Ri $>$ 0), ϕ_h is evaluated by (Arya, 1988),

$$\phi_h = (1 + 5\zeta);\ [\zeta = (\mathrm{Ri}/(1 - 5\ \mathrm{Ri})] \quad (7)$$

In this formulation, the Richardson's number under very stable conditions is set to a limiting value to ensure computational stability. Furthermore, when Ri becomes large at night due to suppressed windspeed, calculations tend to decouple the surface from the overlying atmosphere, and as such unrealistic temperatures are obtained at the ground surface (see also Mahrt and Ek, 1984; Matthias, 1990; Ottoni et al., 1992). In this formulation the Richardson's number under stable conditions is set to a limiting value of 0.1 to ensure computational stability.

Table 1
The prescribed geographic, atmospheric and surface parameters used in the model

Parameter	Unit	January	July
Geographic			
Latitude	Degrees	31	31
Day	Julian	15	200
Atmospheric			
Air temperature			
Mean	K	16	33.2
Diurnal amplitude	K	9	10
Windspeed			
Mean	m s^{-1}	2.8	2.95
Diurnal amplitude	(m s^{-1})	2.5	2.5
Vapor pressure	kPa	1.06	2.02
Surface			
C_w	MJ m^{-3} K^{-1}	4.18	4.18
C_g	MJ m^{-3} K^{-1}	1.7	1.7
K_w	W m^{-1} K^{-1}	0.8	0.8
z_o	m	0.01	0.01
a_p	Dimensionless	0.12	0.10
a_g	Dimensionless	0.20	0.20
ε_g	Dimensionless	0.95	0.95
ε_w	Dimensionless	0.97	0.97

3. Calculation of heat conduction

Lateral heat conduction across the pan boundary (Q_C) is evaluated by solving the two-dimensional heat diffusion equation of the soil adjacent to the pan, assuming a homogeneous medium,

$$\frac{\partial T}{\partial t}=\alpha\left(\frac{\partial^2 T}{\partial x^2}+\frac{\partial^2 T}{\partial z^2}\right) \tag{8}$$

where α is thermal diffusivity ($m^2\ s^{-1}$). Eq. (8) is solved with the appropriate boundary conditions described below. The energy balance equation is solved at the upper boundary ($i = 1$, $j = 1$, n),

$$S(1-a_g)+L_D-\varepsilon_g\sigma T_{sj}^4-Q_{Hj}-G_j=0 \tag{9}$$

where a_g is ground albedo, ε_g is ground emissivity, T_{sj} is the skin temperature of the jth surface node, Q_{Hj} and G_j are the corresponding expressions for sensible heat and heat conduction from the jth surface node. In this formulation, the surface is assumed dry, and thus latent heat flux across the surface–atmosphere boundary is neglected. This assumption is quite realistic considering the aridity of this site. At the bottom boundary, 1.5 m below the surface ($i = n$; $j = 1$, n), heat conduction is assumed to be zero,

$$K_w\frac{dT}{dz}=0 \tag{10}$$

where K_w is thermal conductivity ($W\ m^{-1}\ K^{-1}$). Heat flux in the x direction 1 m away from the outer edge of the pan ($i = 1$, n; $j = 1$) is assumed as zero. The temperature distribution within the soil profile 1 m away from the pan is obtained by solving the heat diffusion equation (in the z direction only) with the surface energy balance equation at the upper boundary and a zero heat flux 1.5 m below the surface; this profile is taken as the left-hand boundary. Because of symmetry, the heat diffusion equation is solved in one direction only. The pan, which represents the fourth boundary, is assumed isothermal at a given time step.

4. Initial conditions and model integration

The model is integrated using average meteorological conditions encountered at the southern edge of the Dead Sea during January and July. Table 1 presents the prescribed surface and atmospheric forcings employed in the model. Windspeed and air temperature are prescribed from observational values using Fourier series, such that their minima and maxima occur at 0500 and 1400 local time (utc + 2 h), respectively. In this paper, thermal conductivity is taken as $0.8\ W\ m^{-1}\ K^{-1}$. This value is larger than what is reported in the literature for dry soils. However, soils near pans are compact due to perturbation resulting from repeated human activities. During January, short and longwave radiation fluxes reaching the surface are adjusted in order to take into account the effect of cloud cover. In this month, solar radiation reaching the surface is around $10\ MJ\ m^{-2}\ day^{-1}$, which gives an average atmospheric transmission of about 50%. During July, however, no adjustment was needed because of persistently clear skies prevailing in this environment. The initial soil temperature within the various profiles was assigned the long-time observed average value at 1.0 m below the surface.

To solve for temperature distribution within the soil plane, the temperatures of the upper boundary nodes are solved. This boundary consists of 10 non-linear coupled energy balance equations,

$$\begin{aligned}S(1-a_g)+L_D-\varepsilon_g\sigma {T_{1,j}^n}^4-Q_{Hj}\\ -\left(K_w/\Delta z\left(T_{1,j}^n-T_{i+1,j}^{n-1}\right)\right)\\ -K_w/\Delta x\left(2T_{1,j}^n-\left(T_{1,j-1}^n+T_{i,j+1}^n\right)\right)=0\end{aligned} \tag{11}$$

The resulting equations are iteratively solved using Newton's algorithm. The iteration was terminated when the difference in the sum of consecutive iterations ($|\sum_{j=10}^{10} T_j^k - T_j^{k-1}|$) is less than 0.1 K; where T_j^k and T_j^{k-1} represent current and previous iterations, respectively. A convergence was usually attained after 5–8 iterations.

The temperature distribution of the interior nodes (Eq. (8)) is obtained by an explicit finite difference form (see Barakat and Clark, 1966):

$$\begin{aligned}\left(T_{i,j}^{n+1}-T_{i,j}^n\right)/(\Delta t)=\alpha/\Delta x^2\left(T_{i,j-1}^n+T_{i,j+1}^n+T_{i+1,J}^n\right.\\ \left.+T_{i-1,j}^n-4T_{i,j}^n\right)\end{aligned} \tag{12}$$

The nodal width of Δx and Δz were assumed equal, 0.1 m each, and Δt is the time step. A 10-min time step is used in the present model. Unconditionally

stable solution is obtained when $(\Delta t\alpha(1/(\Delta x)^2 + 1/(\Delta z)^2 < 0.5)$. In this calculation, the right-hand boundary (pan temperature), which is determined by solving Eq. (1) iteratively, is taken from the previous time step; this has a negligible effect on the calculations because pan temperature varies very little with time. The present model is integrated until two consecutive diurnal cycles reproduce identical results; this is achieved after about 6 diurnal cycles in July and 10 cycles in January.

5. Results and discussion

5.1. Model results

For verification purposes, soil temperatures were calculated and compared to long-term observations obtained in a meteorological station located several kilometers from the sunken pan (Fig. 2). The model slightly underestimates the subsurface temperature, particularly in winter. This may be a result of the timing of the observations; the calculated temperatures represent the average of the hourly values whereas the observed ones are the averages of three readings taken at 0800, 1400 and 2000 local time. These observations are expected to overestimate soil temperatures, particularly for the upper soil nodes, which respond more rapidly to surface heating. Other sources of uncertainty may be linked to the parameterization of certain elements such as downcoming longwave radiation, surface roughness and/or wind speed. Uncertainty of any of these parameters could contaminate the results. The differences between calculated and observed soil temperatures, however, are quite small, ranging from 0.5 to 2 K. Additionally, pan temperature and evaporation rates calculated by the model are very similar to the observed values during both January and July. Calculated daily pan evaporation in January and July are 3.66 and 13.51 mm which are very close to the long-term (5 years) observed values of 3.61 and 13.76 mm, respectively. Calculated and observed pan temperatures during January are 13.7 and 13.5 K, and during July are 27.7 and 28.35 K, respectively. These results suggest that the model is able to reproduce credible results.

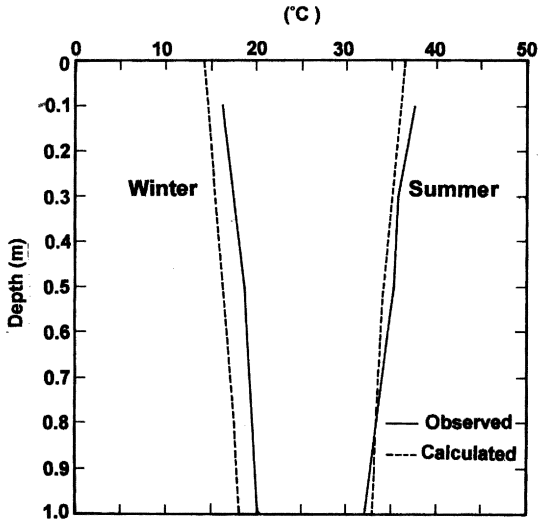

Fig. 2. Calculated average daily soil temperatures versus the observed values at the various depths.

5.2. Heat conduction

Heat conduction across the pan–substrate boundary is calculated by

$$Q_C = 2\pi r \Delta z \sum_{i=1}^{9} \left(0.5\left(T_{i,j=n} + T_{i+1,j=n}\right) - T_{pan}\right) + \frac{K_w}{\Delta z}\left(T_{pan} - T_D\right) \quad (13)$$

where r is radius of the pan, and T_{pan} is the temperature of the pan. Heat conduction across the bottom of the pan (the second term in Eq. (13)) is approximated using the temperature difference between the average daily temperature of the pan and the 'deep' soil; this is approximated to be about 5 W m^{-2}.

Fig. 3 illustrates the temperature field close to the sunken pan during two diurnal cycles, one in January and the other in July. Except for the early morning hours when the top soil layer is slightly cooler than the pan, the soil temperature is always higher than that of the pan, signifying a positive heat flow across the pan–soil boundary. The temperature difference between the sunken pan and the surrounding soil column reaches more than 20 K near the surface at 1300 in summer. The soil temperature, particularly near the surface, has a strong diurnal trend, whereas the pan temperature was changing quite slowly. For instance, the diurnal temperature amplitude of the bare soil

exceeds 30 K, whereas the corresponding value for the pan was about 3 K. These variations reflect the differences in the heat capacity and the mode of net radiation partitioning over the two media.

Model results indicate that heat conduction across the boundary of the sunken pan is larger in summer than in winter. This feature is linked to the greater temperature difference between the sunken pan and the adjacent soil in summer. Total diurnal heat fluxes across the pan–substrate boundary are approximately 1.06 and 2.15 MJ m^{-2} in January and July, respectively. Pan temperature with heat conduction across the pan–soil boundary is warmer than that without conduction by about 0.4 K in July and in January. Although heat conduction in winter is smaller than that in summer, the temperature difference resulting

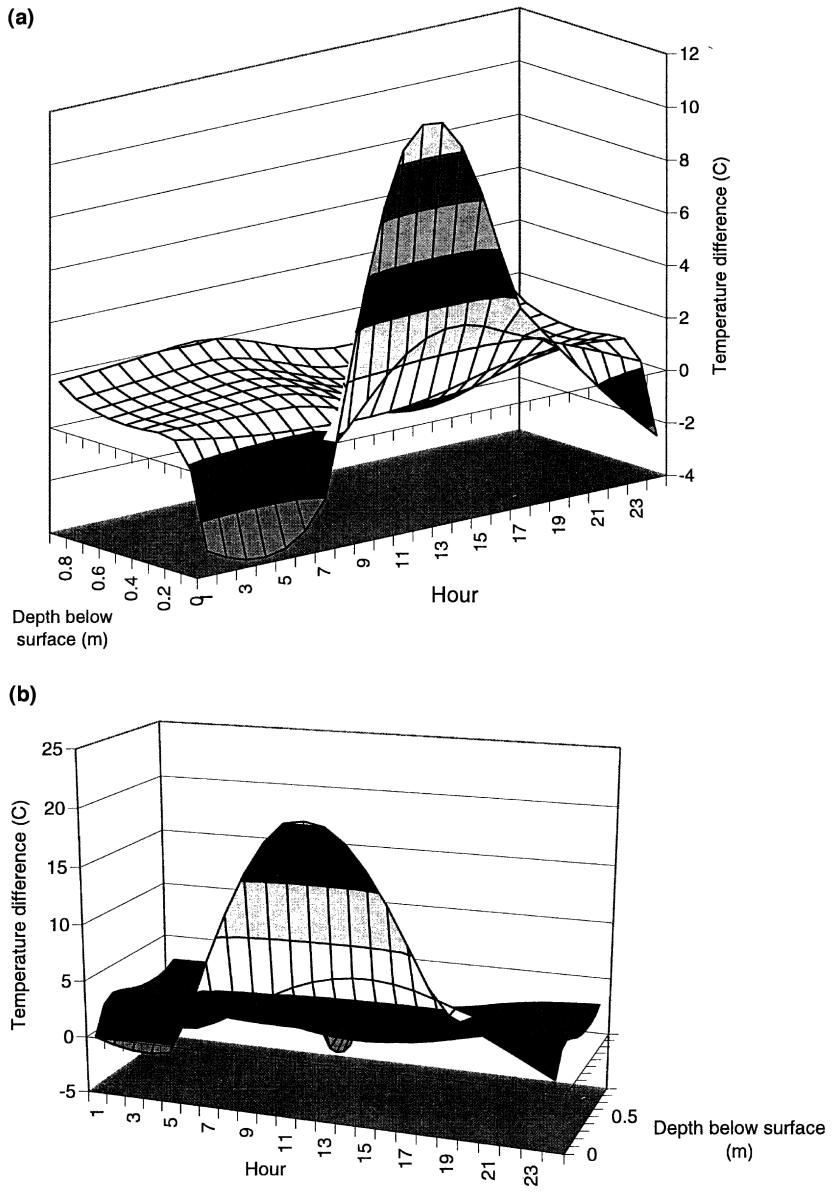

Fig. 3. Diurnal temperature difference between the sunken pan and the adjacent soil nodes during January (a) and July (b).

from heat conduction is practically identical in both seasons. This is attributed to the low energy levels in winter, which renders the pan temperature quite sensitive to small alterations in heat input.

5.3. Evaporation calculation

Evaporation from the pan is calculated using the Penman equation (see Tetzlaff, 1979; Adams and Tetzlaff, 1989),

$$\lambda E = \Delta((Rn - Q_s - Q_C) + \Psi \rho C_p kh(e_a^* - e_a))/(\Delta + \Psi) \quad (14)$$

where Rn is net radiation, Q_s is change in heat storage within the pan, Q_C is heat conduction calculated from Eq. (13), Δ is the slope of saturation vapor pressure calculated from water and air temperatures and vapor pressures, Ψ is the psychrometric constant, e_a^* is saturation vapor pressure at air temperature, e_a is ambient vapor pressure, and kh is the aerodynamic term (see Eqs. (4) and (5)). Unlike Eq. (5), the Penman equation includes both the energy and the aerodynamic terms, and as such it provides a method for calculating evaporation due to energy availability and aerodynamic terms separately (see also Tetzlaff, 1979; Shuttleworth, 1983; Adams and Tetzlaff, 1989).

Comparison between evaporation from a large sunken pan (E_S) and a Class A pan (E_P) carried out from 1991 to 1996 at the southern edge of the Dead Sea, a very hot and dry environment, reveals that the mean ratio of E_S/E_P is around 0.8, with a standard deviation of 0.033. Evaporation measurements were carried out every 2 days between 0800 and 0900 (see also Oroud, 1994). Routine check-ups carried out every several months revealed that the sunken pan did not suffer from any leaking problems. Fig. 4 shows monthly evaporation rates from the two pans along with the monthly range.

The calculated total daily evaporation rates in July with and without heat conduction are about 13.5 and

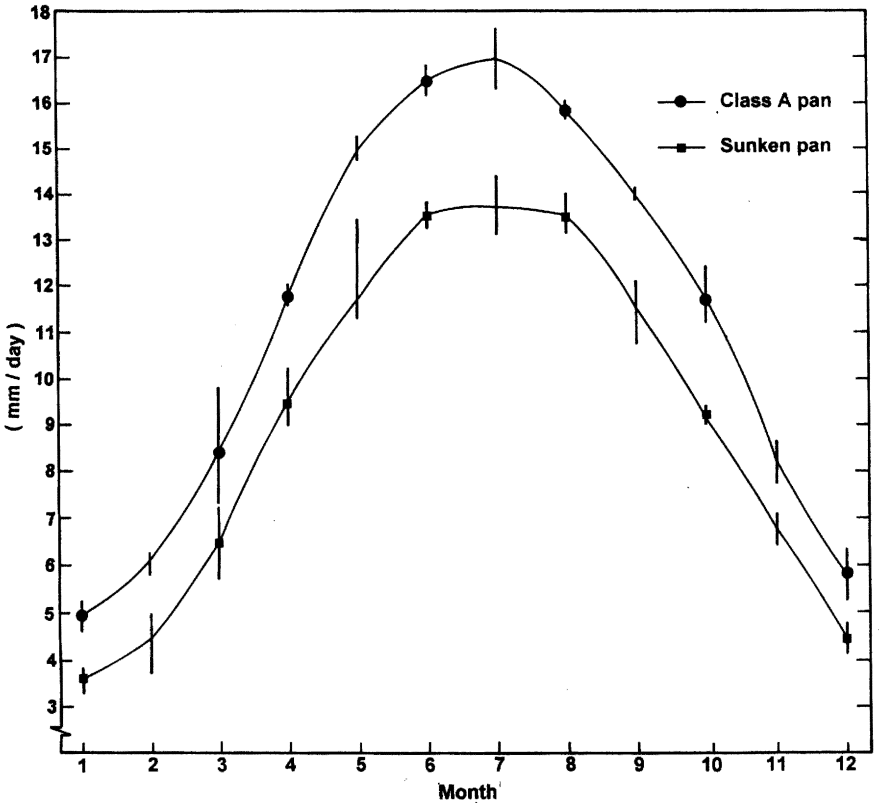

Fig. 4. Mean daily evaporation from a Class A pan and a sunken pan at the southern edge of the Dead Sea in the period 1991–96.

12.8 mm, respectively; corresponding values for January are 3.66 and 3.4 mm, respectively. It appears, therefore, that heat conduction has increased daily evaporation by about 5% (20 mm month^{-1}) in summer and 8% (10 mm month^{-1}) in winter. The ratios of heat conduction to daily net radiation (Q_C/Rn) of the pan are 10 and 34% in July and January, respectively. The above discussion implies that around 7% of total annual evaporation from a sunken pan located in this type of environment is attributed to heat conduction from the surrounding soil profile. These figures illustrate the importance of conduction heat flux across the boundary of a sunken pan in hot, dry environments.

It appears, therefore, that the ratio of E_S/E_P without conduction would be around 0.75, compared to the actual observed value of 0.8. Assuming that lake to Class A pan evaporation ratio (E_L/E_p) in this environment equals 0.6, a conservative value, we would conclude that the ratio of lake to sunken pan evaporation ((E_L/E_P)/(E_S/E_P)) is around 0.75. This figure is smaller than that reported by Kohler (1954) and Hounam (1973) who gave a value close to 0.9 (see also Brutsaert, 1982, p. 253). The ratio which is suggested in this paper would lead to an evaporation rate from a nearby fresh, shallow lake of 2450 mm year^{-1}, which is close to the values obtained by Stanhill (1969) for Lake Tiberias in the northern Jordan Valley and Omar and El-Bakry (1981) for Lake Naser in Southern Egypt.

5.4. Pan and shallow lake evaporation

The above discussion can be extended to tentatively illustrate the difference in evaporation between a sunken pan and a shallow lake/dam, where moisture modification of an airmass passing over the latter is insignificant. Kohler (1954) and Hounam (1973) indicated that daily net radiation over a shallow lake and a deep sunken pan are not different; this is essentially true because water temperature and albedo of both media are very close to each other. Additionally, diurnal heat storage terms for both media are expected to be close to zero, particularly when rapid weather fluctuations do not occur. Given the above assumptions, evaporation attributed to energy and aerodynamic terms for a sunken pan and a shallow lake can be derived. Evaporation attributed to net radiation for a sunken pan and a shallow lake can be expressed by,

$$\Delta(Rn_p - Q_C)/(\Delta + \Psi) \cong \Delta Rn_L/(\Delta + \Psi) \quad (15)$$

where the subscripts p and L stand for a sunken pan and a shallow lake, respectively. Using average July meteorological values of air temperature, pan temperature, downcoming radiation and vapor pressure, we find that evaporation from a shallow water body due to net radiation would be about 7.2 mm day^{-1}. During this month, the observed average evaporation from a sunken pan is 13.76 mm day^{-1}. Using the lake/sunken pan ratio suggested in the preceding section (0.75), evaporation from a nearby shallow lake would be close to 10.3 mm day^{-1}. Thus, the aerodynamic term in the Penman equation for the sunken pan and the shallow lake would be around 5.9 (13.06–7.2) and 3.1 mm day^{-1}, respectively. Therefore, net radiation accounts for about 52 and 70% of evaporation from a sunken pan and a shallow lake in July; corresponding values for the aerodynamic terms account for 43 and 30%. The remaining 5% for the sunken pan are due to conduction heat flux. It appears, therefore, that the main difference in evaporation between a shallow lake and a sunken pan in summer is largely due to differences in surface roughness of the two media.

Analysis by Morton (1983a, p. 25), Morton (1983b, p. 83) and Shuttleworth (1983) suggest that transfer coefficients over land surfaces are larger than those encountered over a shallow lake. Additionally, Kohler (1954) reported that wind speeds recorded over a Class A pan located in an open site was smaller than that recorded over Class A pans situated in sites with obstructions. As a result, evaporation from pans situated in the open site was smaller by about 4%. This is likely due to the higher gustiness near the surface of the pan compared to that over a lake surface due to the presence of a horizontal temperature gradient between the pan and the surrounding terrain. This situation is favorable for convection to develop, and as such increases the occurrence of gustiness. The above finding is supported further when examining E_L/E_S in humid environments. In these regions the drying power of air is small which renders the second term in the Penman equation rather small, and thus evaporation from both media is controlled more or less by energy availability. Under such conditions the ratio

of lake to sunken pan evaporation would be close to unity, as suggested by Kohler (1954) and Hounam (1973). The above discussion indicates that evaporation from a sunken pan located in humid environments would very likely resemble that from a shallow lake. In dry, hot environments, evaporation from a sunken pan would overestimate that from a nearby shallow lake/dam as a result of differences in the drying power of air on one hand, and lateral heat conduction on the other.

6. Conclusion

Heat conduction across the boundary of a large sunken pan located in a hot, dry environment is evaluated using a numerical procedure. Calculations indicate that around 5–8% of annual evaporation from this pan is attributed to this additional heat source. Slight differences in saturation vapor pressure over the lake and the pan could also affect evaporation from the two media. The contributions of energy availability and aerodynamic terms to evaporation from a sunken pan and a shallow lake are also illustrated. Calculations carried out in summer indicate that evaporation from a shallow lake is primarily controlled by energy availability due to a reduced surface roughness, whereas evaporation from a sunken pan is controlled equally by energy availability and the aerodynamic term. Molecular heat conduction across the pan–substrate boundary appears to be important in increasing evaporation from sunken pans in hot, arid environments.

References

Adams, L.J., Tetzlaff, G., 1989. Annual precipitation values at 20N/0E in the early Holocene, Theor. Appl. Climatol., 39, 205–212.

Arya, S.P., 1988. Introduction to Micrometeorology. Academic Press, San Diego, CA.

Asaeda, T., Vu Thanh, C.A., 1993. The subsurface transport of heat and moisture and its effect on the environment: a numerical model, Bound. Lay. Meteorol., 65, 159–179.

Barakat, H.Z., Clark, J.A., 1966. On the solution of the diffusion equation by numerical methods, Trans ASME: J. Heat Transfer, 88, 421–427.

Brutsaert, W., 1975. On a derivable formulae for longwave radiation from clear skies, Water Resour. Res., 11, 742–744.

Brutsaert, W., 1982. Evaporation into the Atmosphere. Reidel, Dordrecht, Holland.

Doll, D., Ching, J., Keneshiro, J., 1985. Parameterization of subsurface heating for soil and concrete using net radiation data, Bound. Lay. Meteorol., 32, 351–372.

Ferguson, H.L., den Hartog, G., Louie, P.Y.T., 1985. Estimation of shallow lake evaporation using Class A pan. In: Casebook on Operational Assessment of Areal Evaporation. WMO-no. 653.

Grant, R.F., Izaurralde, R.C., Chanasky, D.S., 1995. Soil temperature under different surface managements: testing a simulation model, Agric. Forest. Meteorol., 73, 89–113.

Holtslag, A.A., Van Ulden, A.P., 1983. A simple scheme for daytime estimates of the surface fluxes from routine weather data, J. Clim. Appl. Meteorol., 22, 517–529.

Hounam, C.E., 1973. Comparison between Pan and Lake Evaporation. WMO technical note no. 126, Geneva, Switzerland.

Idso, S.B., Asae, J.K., Jackson, R.D., 1975. Net radiation–soil heat flux relations as influenced by water content variations, Bound Layer Meteorol., 9, 113–122.

Iqbal, M., 1983. An Introduction to Solar Radiation. Academic Press, New York.

Kimball, B.A., 1981. Rapidly convergent algorithm for non-linear humidity and thermal radiation terms, Trans. of the ASAE, 24, 1476–1477.

Kohler, M.A., 1954. Pan evaporation: water loss investigations: Lake Hefner. US Geological Survey. Professional paper no. 269, pp. 127–148.

Loomis, L.Y., Hsiao, R.S., 1992. Simulation of soil temperature in crops, Agric. Forest Meteorol, 61, 23–38.

Mahrt, L., Ek, M., 1984. The influence of atmospheric stability on potential evaporation, J. Climate Appl. Meteorol., 23, 222–234.

Matthias, A.D., 1990. Simulation of daily energy budget and mean soil temperatures at an arid site, Theor. Appl. Climatolo., 42, 3–17.

Morton, F.I., 1983. Operational estimates of areal evapotranspiration and their significance to the science and practice of hydrology, J. Hydrolo., 66, 1–76.

Morton, F.I., 1983. Operational estimates of lake evaporation, J. Hydrolo., 66, 77–100.

Omar, M.H., El-Bakry, M.M., 1981. Estimation of evaporation from the Aswan High Dam (Lake Naser) based on measurements over the lake, Agric. Meteorol., 23, 293–308.

Oroud, I.M., 1994. Evaluation of saturation vapor pressure over hypersaline solutions at the southern edge of the Dead Sea, Jordan. Sol. Energy, 53, 497–503.

Ottoni, T., Matthias, A.D., Guerra, A.F., Slack, D.C., 1992. Comparison of three resistance methods for estimating heat flux under stable conditions, Agric. Fores. Meteorol., 58, 1–18.

Paltridge, G.W., Platt, C.M., 1976. Radiative Processes in Meteorology and Climatology. Elsevier Science, Amesterdam.

Sellers, W.D., 1965. Physical Climatology. University of Chicago Press, Chicago, IL.

Shuttleworth, W.J., 1983. Evaporation models in the global water budget. In: A. Street-Perrot, M. Beran, R. Ratcliffe (Eds.), Variations in the Global Water Budget, Reidel, Dordrecht, pp. 147–171.

Stanhill, G., 1969. Evaporation from Lake Tiberias: an estimate by the combined water balance–mass transfer approach, Israel. J. Earth Sci., 18, 101–108.

Sweers, H.E., 1976. A nomogram to estimate the heat exchange coefficient of windspeed and temperature: a critical survey of some literature, J. Hydrol., 30, 375–401.

Tetzlaff, G., 1979, The daily cycle of water temperature of a shallow lake. In: W.H. Graff, C.H. Mortimer (Eds.) Developments in Water Science, vol. 11, Hydrodynamics of Lakes. Reidel, Dordrecht, pp. 347–360.

Turk, L.J., 1970. Evaporation of brine: a field study of the Bonneville Salt Flats, Utah. Water Resour. Res., 6, 1209–1215.